Electrochemical study and experimental simulation of the synergistic effect of a formulation based on Ficus pumila Linn. Leaves extract and zinc sulfate on the XC38 steel corrosion inhibition in NaCl solution

Odilon Romaric Wamba-Tchio, Martin Pengou, Anne-Lucie Teillout, Cédric Baumier, Israël-Martyr Mbomekallé, Pedro de Oliveira, Charles Péguy Nanseu-Njiki, Emmanuel Ngameni

Electrochemical study and experimental simulation of the synergistic effect of a formulation based on *Ficus pumila Linn*. leaves extract and zinc sulfate on the XC38 steel corrosion inhibition in NaCl solution

Odilon Romaric Wamba-Tchio [a], Martin Pengou [b], Anne-Lucie Teillout [c], Cédric Baumier [d], Israël Martyr Mbomekallé [c], Pedro de Oliveira [c], Charles Péguy Nanseu-Njiki [a]*, Emmanuel Ngameni [a]

[a] Department of Inorganic Chemistry, University of Yaoundé 1, B.P. 812, Yaoundé, Cameroon

[b] Faculté des Sciences-ENS, Université de Maroua, B.P. 46, Maroua, Cameroon

[c] Institut de Chimie Physique, UMR 8000, CNRS, Université Paris-Saclay, 91405 Orsay Cedex, France

[d] IJCLab, UMR 9012, CNRS, Université Paris-Saclay, 91405 Orsay Cedex, France

Authors' e-mail addresses : *wambaodilon@yahoo.com*, *mapesu@yahoo.fr*, *anne-lucie.teillout@universite-paris-saclay.fr*, *cedric.baumier@csnsm.in2p3.fr*, *israel.mbomekalle@u-psud.fr*, *pedro.deoliveira@u-psud.fr*, *nanseu@yahoo.fr*, *engameni@yahoo.fr*

*Corresponding author at Department of Inorganic Chemistry, University of Yaoundé 1, B.P. 812, Yaoundé, Cameroon. E-mail address: *nanseu@yahoo.fr*

Abstract

The inhibitive activity of a mixture of *Ficus pumila Linn. leaves* hydroalcoholic extracts (HEFP) and zinc ions against corrosion of XC38 steel in NaCl solution was investigated. Electrochemical measurements (potentiodynamic polarization and electrochemical impedance spectroscopy at and around the corrosion potential) and surface analysis (SEM/EDX) have shown that the presence of zinc ions considerably increases the inhibitive capacity of HEFP. However, appropriate concentrations of zinc ions (50 and 100 ppm) and of HEFP (200 ppm) are necessary to have an optimal inhibitive effect. The formation of organometallic complexes between zinc ions and some organic compounds of HEFP (polyphenols and carbohydrates) are the determining step of the synergistic inhibition. Since the main inhibitive agents in plant extracts are polyphenols, a simulation of this inhibitive character was electrochemically done with a mixture of flavonoid (quercetin), phenolic acid (gallic acid) and zinc ions in order to elucidate the inhibition mechanism. The obtained results showed that the electrochemical

behavior of XC38 steel in the presence of this mixture is quite similar to that obtained in the presence of HEFP + Zn^{2+} formulation. The proposed inhibition mechanism, which explains the good inhibitive efficiency observed in presence of the HEFP + Zn^{2+} formulation, is based on concerted reactions between the steel oxidation products (Fe^{2+} and Fe^{3+}), the zinc ions and the Iron(II) and Iron(III) complexing agents present in the extract.

Keywords: Metal-organic complexes, corrosion products, plant extract, potentiodynamic polarization, EIS

1. Introduction

Carbon steel is a widely used material because of its machinability, ductility, high melting point, good thermal and electrical conductivity. However, this material is susceptible to deteriorate due to corrosion processes when it interacts with its environment through an oxidizing agent [1, 2]. In neutral and alkaline environments, the main oxidizing agent is oxygen [3]. If the medium contains chloride ions, steel corrosion is accelerated locally following a localized corrosion mechanism [3-6]. To prevent this insidious and very devastating form of corrosion, the use of corrosion inhibitors is generally recommended. The corrosion inhibitors commonly used for this purpose are synthetic or natural organic compounds having mostly heteroatoms (O, N, P or S) and / or unsaturated rings in their structures [2, 7-10]. These electron-rich sites facilitate their adsorption on the metal surface, generally leading to the formation of a protective film which reduces the steel corrosion rate in chloride medium [11, 12]. For environmental reasons, synthetic inhibitors are gradually replaced by renewable and ecologically solutions such as plant extracts.

Plant extracts have already proved to be very effective against steel corrosion in hydrochloric acid environments, but in neutral and alkaline media their performances are not very often spectacular [9, 11, 13-15]. In fact, they contain organic compounds (flavonoids, tannins and carbohydrates) with excellent chelating properties towards cations resulting from steel oxidation (Fe^{2+} and Fe^{3+} ions) [15-20]. In neutral and alkaline media, these properties are generally responsible of a stimulating effect on the corrosion process thus explaining the low inhibiting efficiencies frequently observed in these cases [7, 21-23]. It has been proved that by combining plant extracts with inorganic compounds such as zinc salts, the corrosion inhibiting efficiency can be significantly improved [9]. The good inhibitive activity is generally attributed to a synergistic effect between zinc ions and some compounds in the extracts with metal ion chelating abilities (such as polyphenolic, amino and carbohydrate compounds) leading to very

stable and protective films on the steel surface, which considerably reduce the corrosion rate [24-31]. Moreover, to the best of our knowledge, almost no work carried out in the field of steel corrosion inhibition by plant extract + Zn^{2+} formulations has focused on the influence of the zinc ion or the extract concentration on the inhibitive performance of formulations [24-27, 32-37]. It is known that the behavior (in terms of adsorption, diffusion and reactivity) at the metal/electrolyte interface of the organometallic species susceptible to form in the presence of plant extracts + Zn^{2+} formulations strongly depends on the concentration of the metal cations and the ligands present [18, 38]. A systematic electrochemical evaluation of the concentration effect of both the metal cations and the plant extracts can provide new arguments concerning the mechanistic aspect of steel corrosion inhibition in NaCl medium by plant extract + Zn^{2+} formulations. In addition, there is still some uncertainty regarding the role of steel oxidation products (Fe(II) and Fe(III)) and the contribution of inhibitive compounds in the extracts during the inhibition process, since some extract inhibitive compounds can chelate Fe(II) and/or Fe(III) ions forming more stable complexes than with Zn^{2+} ions [39]. One interesting approach to clarify these issues would be to evaluate the electrochemical behavior of steel in the presence of formulations based on Zn^{2+} and some active inhibitor compounds contained in the extracts.

Ficus pumila Linn. (FP) is a member of the Moraceae family and commonly found in tropical areas [40]. It has been reported that the leaves of this plant are rich in flavonoids, tannins, terpenoids and carbohydrate glycosides [41, 42]. These different compounds have structural elements (unsaturated rings, nucleophilic oxygen atoms, etc.) that can favor the formation of chelates with metal cations [43]. This property makes FP leaf extracts seriously attractive for the formulation of plant extract-zinc salt composites used to inhibit steel corrosion in near-neutral environments. Based on the literature, extracts of this plant have not yet been used in the field of corrosion inhibition. Their inhibitive action on steel corrosion in NaCl medium and the possible synergistic effect with zinc salts therefore deserves to be investigated.

This work presents a double objective. Firstly, through an electrochemical approach, it will evaluate the inhibitive activity and the inhibitor concentrations effect of a mixture of zinc salt and *Ficus pumila leaves* hydroalcoholic extracts against corrosion of XC38 steel in NaCl solution. Secondly, a simulation of this inhibitive activity will then be performed using a mixture of flavonoid (quercetin), phenolic acid (gallic acid) and zinc ions as inhibitive composition. This will allow a better understanding of the inhibition mechanism when Zn^{2+} and plant extracts formulation are used for corrosion inhibition of carbon steel in NaCl medium. Electrochemical techniques (polarization curves, electrochemical impedance spectroscopy at

and around the corrosion potential) and surface characterizations by SEM coupled with EDX were used to collect useful data needed to achieve these objectives.

2. Experimental

2.1 Material and solutions

The corrosion studies were carried out on a cylindrical sample of XC38 steel purchased from AcierDetailDecoupe and having the following chemical composition (% by mass): 0.36 C, 0.40 Si, 0.68 Mn, 0.045 S, 0.40 Cr, 0.40 Ni, 0.10 Mo, 0.045 P and Fe (balance). For the corrosion rate measurements, the side surface of the XC38 steel rod was coated with polytetrafluoroethylene (PTFE) tape, leaving a free circular basal working area of 78.5 mm^2. To obtain reproducible measurements, this basal surface (working electrode) was abraded on silicon carbide abrasive papers of different grades (500, 1000, 1200 and 2400) from the most to the least abrasive. The corrosive solution (0.1 M NaCl) was prepared with deionized water and NaCl purchased from Scharlau. Zinc salt ($ZnSO_4$. $7H_2O$) was purchased from Sigma-Aldrich. Leaves of *Ficus pumila Linn*. collected in Yaoundé (Cameroon) were used to prepare the hydroalcoholic extract. The extraction procedure is described in the Supplementary Information. According to the literature, the main constituents of this hydroalcoholic extract are flavonoids, tannins and carbohydrate glycosides [40-42]. Solutions containing the plant extract and zinc ions formulations were prepared in corrosive medium with a mixture of different concentrations of plant extracts (100, 200 and 400 ppm) and zinc salt (25, 50, 100 and 200 ppm). All other reagents were of high purity and were used as received without further purification.

2.2 Spectroscopic characterizations of the plant extract and of the plant extract + Zn^{2+} mixture

Fourier-transform infrared spectroscopy (FTIR) analyses were carried out on the dry hydroalcoholic extract. The spectra were recorded on a Bruker Alpha spectrometer, equipped with a DTGS detector in the range of 4000 – 400 cm^{-1} with a resolution of 4 cm^{-1} during data acquisition. A Genesis 10S UV-vis spectrophotometer was used to determine the total polyphenols and flavonoids content in the extract and to get useful data concerning the interaction between the *Ficus pumila* leaves extract and zinc ions. The protocols used for polyphenols and flavonoids quantification are presented in the Supplementary Information.

2.3 Electrochemical measurements

The electrochemical experiments were carried out in a thermostatically controlled electrochemical cell maintained at 20 °C, with three electrodes. The working electrode was an XC38 steel rod prepared for corrosion studies, a platinum wire with 222.9 mm^2 surface area as auxiliary electrode and a saturated calomel electrode (SCE) as reference electrode. These electrodes were connected to a Metrohm Autolab PGSTAT Potentiostat/Galvanostat with an impedance module and controlled by the FRA and the GPES softwares for electrochemical impedance spectroscopy (EIS) and potentiodynamic measurements, respectively. Before recording the EIS and the polarization curves, the working electrode was first immersed in the aggressive solution for 2 hours in the absence and in the presence of controlled amounts of inhibitor in order to reach an equilibrium state necessary for the other electrochemical measurements. The polarization curves were recorded over a potential range of -750 to -100 mV / SCE with a scan rate of 0.5 mV / s. The corrosion current (Icorr) is accurately obtained by computer fitting of the polarization curves around the open circuit potential (OCP) using the EC-Lab V10.40 software (see Supplementary Information). The polarization resistance (Rp) was calculated by taking the reverse of the slope of the current potential curve at ± 30 mV from the corrosion potential [5]. The inhibition percentages related to the measurement of Icorr and Rp were obtained using the following formulas:

$$\eta_{Icorr} = (Icorr' - Icorr) \times 100/Icorr' \quad (1)$$

$$\eta_{Rp} = (Rp - Rp') \times 100/Rp \quad (2)$$

where Icorr' and Rp' are the corrosion current and polarization resistance without the inhibitor, respectively; Icorr and Rp are the corrosion current and polarization resistance in the presence of the inhibitor, respectively.

The EIS curves were recorded at and around the corrosion potential (±50mV) with an amplitude of 10 mV, in the frequency range of 10^4 Hz to 10^{-2} Hz [8, 12, 44, 45]. The EIS curves were fitted using the ZsimpWin 3.21 and the EC-Lab V10.40 softwares to extract the relevant experimental parameters as charge transfer resistance (R_{ct}), CPE parameters related to the electrical double layer (n_{dl} and Q_{dl}), film resistance (R_f) and CPE parameters related to the protective film (n_f, Q_f). The quality of the fitting to an equivalent electrical circuit (EEC) was assessed by the chi-square value [46]. The inhibition percentages related to the polarization resistance were obtained using the following formula:

$$\eta_{Rct} = (Rp - Rp') \times 100/Rp \quad (3)$$

Where Rp' is the polarization resistance without the inhibitor and Rp is the polarization resistance in the presence of the inhibitor. Rp is the sum of the resistances due to charge transfer (Rct) and film (Rf) formation by the inhibitor on the steel surface [47-49].

All the electrochemical manipulations were carried out by triplicate in order to ensure the repeatability of the results.

2.4 Scanning electron microscopy (SEM) and energy dispersive X-ray (EDX) analyses

SEM and EDX analyses were used to study the morphology and the elemental composition of the XC38 steel surface after 5 hours of immersion in 0.1 M NaCl solutions in the absence and in the presence of the inhibitor at the optimal concentration. SEM and EDX analyses were performed on a HYROX SH-3000 microscope equipped with an EDX-BRUKER.

3. Results and discussion

3.1 Spectroscopic characterizations of the plant extract and of the plant extract + Zn^{2+} mixture

The FTIR spectrum of the hydroalcoholic extract of *Ficus pumila Linn.* leaves (HEFP) is presented in Fig. 1a. The relevant peaks at 3270, 2925, 1594, 1389, 1251 and 1042 cm^{-1} reveal the presence of O–H, C=C, C=O, C–O and $–CH_2–OH$ functions of polyphenolic compounds and carbohydrates [50-53].

UV-Vis analysis of the HEFP + Zn^{2+} mixture was carried out in order to determine the interactions between the extract compounds and Zn^{2+} ions. The adsorption spectra (Fig. 1b) of the HEFP and of the HEFP + Zn^{2+} mixture show an intense and broad absorption band between 250 and 300 nm which reflects n–π^* electronic transition of the functional groups (like C=O) of polyphenolics compounds in the HEFP [18, 26, 54]. However, the absorption band on the UV-Vis spectrum of the HEFP + Zn^{2+} mixture is less intense than that of the HEFP. This result reveals the existence of interactions between the extract compounds and zinc ions, which probably correspond to electron transfers between heteroatoms such as oxygen and vacant s orbitals of the zinc ions. Indeed, the HEFP contains phenolic compounds such as flavonoids, tannins and phenolic acids capable of chelating Zn^{2+} ions by formation of coordination bonds [55, 56]. This reactivity would therefore justify the decrease in the absorption peak relating to the n–π^* transition in the presence of the mixture.

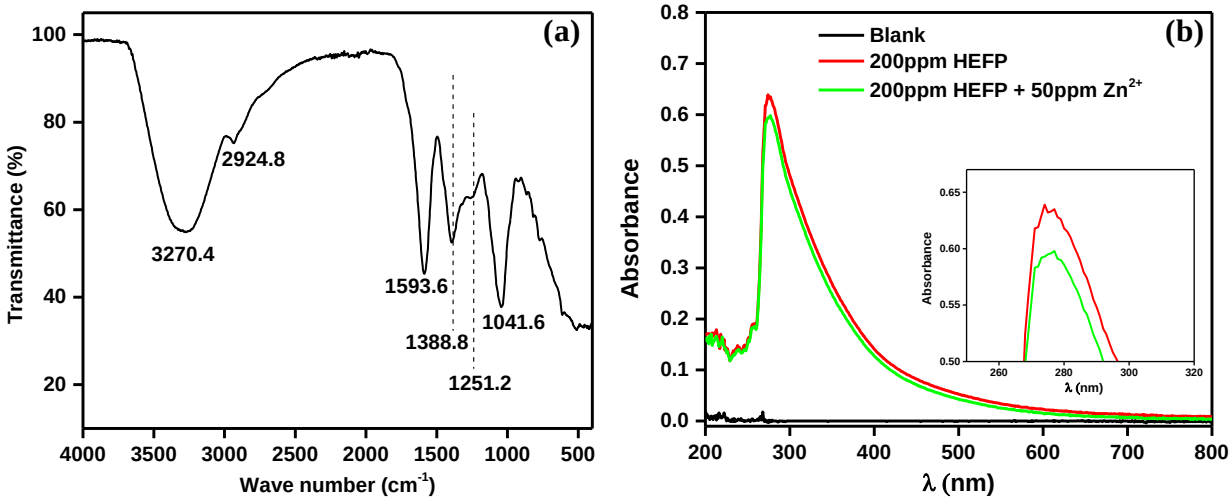

Fig. 1. FTIR spectrum of the HEFP and UV-Vis spectra of the 0.1M NaCl solution containing the HEFP and a formulation of HEFP + Zn^{2+}.

The contents of polyphenol and total flavonoids in the HEFP after quantification (see Supplementary Information) are respectively 166,381 mg GAE /g DE (GAE: gallic acid equivalent, DE: dry extract) and 133.450 mg QE / g DE (QE: quercetin equivalent, DE: dry extract). This information confirms the results obtained by the FTIR and the UV-Vis analyses.

3.2 Evaluation of the corrosion inhibitive activity of the of the plant extract + Zn^{2+} mixture

The corrosion inhibitive capacities of the HEFP + Zn^{2+} mixture were evaluated by linear polarization, EIS (at and around the corrosion potential) and surface analyzes. For comparison purposes, the inhibitive capacities of the HEFP and of $ZnSO_4$ will be also briefly presented.

3.2.1 Potentiodynamic linear polarization

The polarization curves obtained in the absence of the inhibitor (blank), in the presence of the HEFP, in the presence of Zn^{2+} and in the presence of the HEFP + Zn^{2+} mixture are shown in Figs. 2a, 2b, 2c and 2d, respectively. The electrochemical parameters (corrosion potential (Ecorr), corrosion current (Icorr), anodic (βa) and cathodic (-βc) Tafel slopes)) obtained from these curves are presented in Table 1.

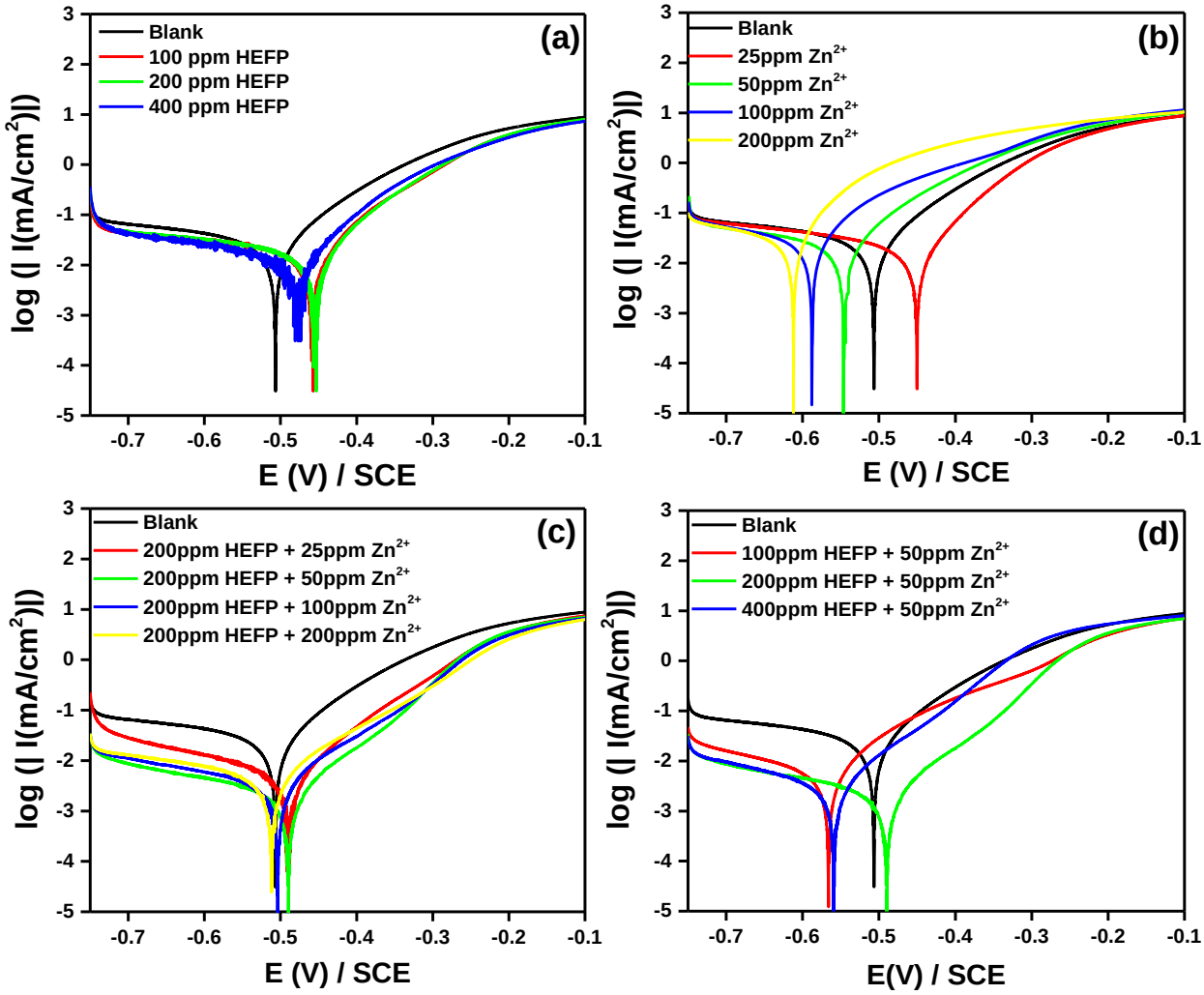

Fig. 2. Polarization curves of XC38 steel in 0,1M NaCl solution in the absence of the inhibitor (Blank), in the presence of the HEFP (a), in the presence of Zn^{2+} (b) and in the presence of the HEFP + Zn^{2+} formulations (c and d).

The presence of the HEFP causes a slight decrease of the anodic and the cathodic currents (Fig.2a), and a low anodic displacement of the polarization curves relative to the control (blank). For 100, 200 and 400 ppm of extract, the respective inhibition percentages obtained are 33.9 %, 39.9 % and 42.4 % with respect to Icorr, and 36.6%, 41.3% and 45.6% with respect to Rp. These low inhibition percentages reflect a low adsorption on the steel surface of the compounds found in the extract in these experimental conditions. Indeed, a good corrosion inhibition of a metal by organic compounds is obtained when the latter adsorb quantitatively on the metal surface to form a stable and sufficiently protective film [2, 22]. The HEFP contains phenolic acid, flavonoids and tannins which are known to form slightly soluble and stable complexes with iron oxidation products (Fe(II) and Fe(III)) [17, 18, 24]. This reactivity could

have a stimulating effect on the corrosion process and would also justify the low inhibition percentage obtained in the presence of the HEFP alone, since these complexes would not form near the steel surface [7, 21, 22].

Table 1. Kinetic parameters obtained from the polarisation curves of XC38 steel in 0,1M NaCl solution in the absence of the inhibitor (blank), in the presence of the HEFP, in the presence of Zn^{2+} and in the presence of the HEFP + Zn^{2+} formulations.

HEFP Concentration (ppm)	Zn^{2+} Concentration (ppm)	Ecorr (mV/ECS)	Icorr ($\mu A.cm^{-2}$)	β_a (mV/dec)	$-\beta_c$ (mV/dec)	Rp ($Ohm.cm^2$)	η_{Icorr} (%)	η_{Rp} (%)
0	0	-508 ± 4	24.3 ± 1.9	99.7 ± 31.	404.7	1117 ± 107	-	-
	25	-452 ± 4	19.5 ± 0.5	81.4 ± 1.2	463.3 ± 7.1	1421 ± 12	19.8 ± 1.6	21.4 ± 0.7
	50	-547 ± 13	23.5 ± 1.0	105.1 ± 8.4	479.3 ± 25.9	1191 ± 45	3.3 ± 4.1	6.2 ± 3.4
	100	-590 ± 8	25.8 ± 0.8	96.0 ± 9.6	350.0 ± 17.2	876 ± 16	-	-
	200	-615 ± 16	30.9 ± 1.3	95.5 ± 4.2	311.6 ± 21.0	659 ± 49	-	-
100	0	-460 ± 18	16.1 ± 1.2	92.4 ± 2.2	498.8 ± 16.2	1763 ± 98	33.9 ± 4.8	36.6 ± 3.4
	25	-505 ± 12	6.3 ± 0.3	99.1 ±1.0	310.3 ± 4.8	4445 ± 77	74.0 ± 1.2	74.5 ± 0.8
	50	-568 ± 5	6.3 ± 0.1	127.3 ± 0.6	270.3 ± 8.5	4358 ± 82	74.0 ± 0.3	74.4 ± 0.4
	100	-500 ± 10	5.9 ± 0.1	105.0 ± 0.4	345.0 ± 10.1	4940 ± 43	75.7 ± 0.4	77.4 ± 0.2
	200	-503 ± 8	7.0 ± 0.5	90.9 ± 1.7	409.5 ± 18.1	3520 ± 105	71.2 ± 2.1	68.3 ± 0.9
200	0	-456 ± 4	14.6 ± 0.3	85.4 ± 0.1	425.4 ± 5.9	1903 ± 79	39.9 ± 1.3	41.3± 4.2
	25	-490 ± 4	5.7 ± 0.2	97.6 ±2.9	309.9 ±11.0	5347 ± 55	76.5 ± 0.9	79.1 ± 0.2
	50	-491 ± 16	2.1 ±0.1	96.5 ± 3.7	344.8 ± 15.8	11906 ± 173	91.3 ± 0.5	90.6 ± 0.4
	100	-505 ± 3	2.7 ± 0.1	94.5 ± 1.8	307.3 ± 20.9	8062 ± 106	88.9 ± 0.5	86.1 ± 0.2
	200	-513 ± 7	5.0 ± 0.2	120.1 ± 1.3	455.0 ± 14.3	6169 ± 88	79.4 ± 0.8	81.9 ± 2.8
400	0	-478 ± 6	14.0 ± 0.6	91.4 ± 0.5	456.4 ± 5.2	2033 ± 65	42.4 ± 2.5	45.1 ± 1.7
	25	-509 ± 11	13.3± 0.4	111.0 ± 4.2	316.4 ± 17.3	2174 ± 51	45.3 ± 1.7	48.6 ± 1.2
	50	-560 ± 4	3.1± 0.2	95.1 ± 2.3	285.5 ± 8.3	7746 ± 74	87.4 ± 0.7	85.6 ± 1.8
	100	-542 ± 7	3.4± 0.2	94.7 ± 2.0	327.7 ± 10.4	7546 ± 71	86.0 ± 0.8	85.2 ± 0.1
	200	-550 ± 5	3.3± 0.1	101.7 ±1.9	358.4 ± 5.7	7743 ± 76	86.4 ± 0.2	85.6 ± 0.1

In the presence of Zn^{2+} used as the sole inhibitor (Fig. 2b), the decrease of the anodic and the cathodic currents are not really noticeable for all the tested concentrations (25, 50, 100 and 200 ppm). The obtained inhibition percentages show that Zn^{2+} is a very poor corrosion inhibitor when used in these conditions. A cathodic shift of the corrosion potential is recorded for all the tested concentrations of Zn^{2+} except in the presence of 25ppm. This reflects a very strong effect of the zinc ions on the cathodic reaction mechanism of corrosion. Zinc ions are actually recognized as cathodic inhibitors [53]. When the local pH is favorable, they have the possibility to form a $Zn(OH)_2$ deposit by reaction with OH^- ions produced during the reduction of

dissolved oxygen on the steel surface [24, 25, 27, 36]. However, the formation of this deposit, which only occurs at the cathodic sites of the corrosion process, does not reduce the overall corrosion rate for the Zn^{2+} ion concentrations tested. A similar observation has been reported [33].

The influence of Zn^{2+} on the corrosion inhibitive activity of the HEFP is presented in Figs. 2c and 2d. In Fig. 2c, the effect of a fixed Zn^{2+} concentration (50 ppm) associated with different extract concentrations was presented in order to highlight the influence of the extract concentration on the inhibitive activity of the HEFP + Zn^{2+} formulations. Fig. 2d shows the polarization curves obtained for an extract concentration of 200 ppm associated with different Zn^{2+} concentrations; this was done in order to determine the influence of Zn^{2+} concentration on the inhibitive capacity of the HEFP + Zn^{2+} mixture.

The presence of zinc ions significantly improves the corrosion inhibitive performance of the HEFP (Figs. 2c and 2d). An important decrease of the cathodic and the anodic currents coupled to a low shift of corrosion potential (less than 85 mV/SCE when compared to the blank) are observed in the presence of the HEFP + Zn^{2+} mixture. This suggests the existence of a mixed inhibitor character of this formulation and the formation of a protective film on the steel surface [8, 24, 31]. A rapid increase of the current with the potential is visible on the anodic branches between -0.35 and -0.25 V/SCE. This behavior is related to a destruction of the protective film by relaxation of the adsorbed compounds on steel surface [57]. The desorption phenomenon was not noticeable when the extract was used alone (Fig. 2a), showing that the zinc ions promote a quantitative adsorption of the HEFP inhibitive compounds [9].

The formulations consisting of 200 ppm HEFP + 50 ppm Zn^{2+} and 200 ppm HEFP + 100 ppm Zn^{2+} give rise to the highest current drops (91.3 and 88.9% respectively with respect to Icorr). For extract concentrations below or above 200 ppm, the inhibition percentages are lower than 91.3 %. Actually, some of the HEFP compounds such as polyphenolic species and carbohydrates have the ability to chelated zinc ions [19]. When the extract concentration necessary to fix the amount of Zn^{2+} present in solution is not reached or is largely exceeded, the synergistic mechanism is no longer optimal. This means that the complexes formed between the compounds present in the extract and the zinc ions are responsible for the synergistic effect observed in the presence of the HEFP + Zn^{2+} formulations. A slightly variation of the anodic Tafel slopes (βa) is observed in the presence of the HEFP + Zn^{2+} mixture compared to the value obtained in the absence of the inhibitor (99.7 mV/decade). On the other

hand, the cathodic Tafel slopes (-βc) decrease considerably in the presence of the HEFP + Zn^{2+} compared to the control. This double observation would reflect the fact that the synergy of action between the compounds in the HEFP and Zn^{2+} ions would have a very marked effect on the cathodic reaction [48].

3.2.2 Electrochemical impedance spectroscopy

The Nyquist and the Bode diagrams of the XC38 steel in the absence and in the presence of the HEFP are shown in Figs. 3a and 3b, respectively. The Bode phase diagram in the absence of HEFP shows a single time constant with a phase angle less than 50° (44.6°), in line with the presence of a flattened capacitive loop observed on the correspondent Nyquist diagram. This observation confirms the formation of a porous and non-uniformly distributed layer on the steel surface by corrosion products [58]. In the presence of the HEFP, two time constants are visible on the Bode diagrams, one at high frequency (110 Hz) not very well defined and characteristic of the relaxation process of the film formed on the metal surface, and the other at low frequency (54.3 mHz) assigned to the electrical double layer [22, 57, 59]. The fact that these two time constants are not very close in terms of frequency would probably mean that the film formed does not adhere well to the metal surface. In addition, the poor phase angles of these two time constants (lower than 50°) reflects the fact that the film formed under these conditions is not sufficiently protective [58]. Two equivalent electrical circuits (EECs) were used to obtain the electrochemical parameters from the Nyquist curves and they show a very good fitting of the experimental data (chi-square of the order of 10^{-4}). The first EEC (Fig. 4a) contains a single time constant and the second (Fig. 4b) has two time constants, in line with the Bode phase diagrams. The electrochemical data (charge transfer resistance (R_{ct}), the constant phase element (CPE) parameters related to the electric double layer (n_{dl} and Q_{dl}), the film resistance (R_f) and the CPE parameters related to the film (n_f, Q_f)) obtained from these EIS analyses are presented in Table 2. A slight increase in Rct is observed in the presence of the HEFP when compared to the blank. Low inhibition percentages of 45.8, 49.9 and 56.7 % are obtained in the presence of 100, 200 and 400 ppm of HEFP, respectively, thus confirming the poor inhibitive character of the HEFP.

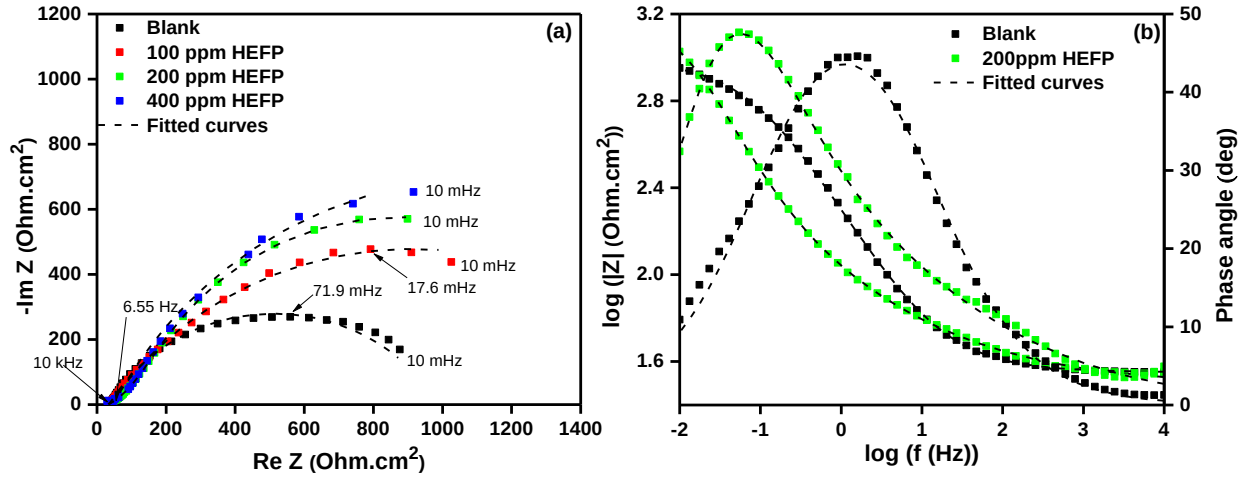

Fig. 3. Nyquist (a) and Bode (b) curves for the XC38 steel in 0.1M NaCl solution in the presence and in the absence of HEFP.

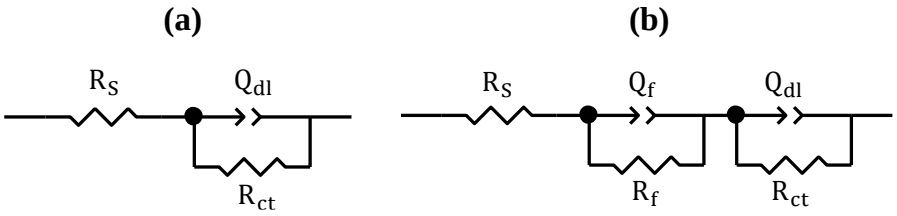

Fig. 4. Equivalent electrical circuits (EECs) used to model the metal-electrolyte interface in the absence (a) and in the presence (b) of the HEFP.

Table 2. Electrochemical parameters of the XC38 steel in 0,1M NaCl solution in the absence and in the presence of the HEFP.

Concentration	R_{ct} (Ohm.cm^2)	n_{dl}	$Q_{dl} \times 10^{-3}$ (Ω^{-1}.cm^{-2}.s^{ndl})	R_f (Ohm.cm^2)	n_f	$Q_{dl} \times 10^{-3}$ (Ω^{-1}.cm^{-2}.s^{nf})	Rp (Ohm.cm^2)	η_{Rp} (%)
Blank	951.9 ± 60.1	0.676 ± 0.014	1.476 ± 0.059	-	-	-	951.9 ± 60.1	-
100 ppm HEFP	1751.0 ± 38.8	0.637 ± 0.005	2.909 ± 0.018	5,7 ± 1.6	0.550 ± 0.025	3.906 ± 0.078	1756.7 ± 40.4	45.8 ± 2.0
200 ppm HEFP	1878.0 ± 52.4	0.819 ± 0.007	4.661 ± 0.049	23.1 ± 2.3	0.546 ± 0.038	3.224 ± 0.709	1901.1 ± 54.7	49.9 ± 1.4
400 ppm HEFP	2186.0 ± 126.8	0.723 ± 0.119	5.518 ± 1.931	12.1 ± 1.9	0.641 ± 0.028	4.490 ± 0.243	2198.1 ± 128.4	56.7 ± 2.4

The Nyquist and the Bode curves of the XC38 steel in the presence of the HEFP + Zn^{2+} mixture are shown in Figs. 5a, 5b, 5c and 5d. Nyquist diagrams show flattened capacitive loops whose diameters increase considerably when the HEFP and Zn^{2+} mixture is present (Figs 5a and 5b). The distorted shape present at the high frequency part of these diagrams can be attributed to the formation of a protective layer on the metal surface [60, 61]. Indeed, an immersion time of

2 h would not be sufficient to show the occurrence of a clear loop in the high-frequency domain. The evolution of the capacitive loop diameters reflects the improvement of the steel resistance against corrosion in the presence of the formulation, which can be confirmed on the Bode diagram by the significant increase of the impedance modulus at low frequency compared to the control [48]. The largest diameters and characteristic phase angles (above 50°) observed for the formulations 200 ppm HEFP + 50 ppm Zn^{2+} and 200 ppm HEFP + 100 ppm Zn^{2+} confirm a greater reduction of the corrosion rate under these conditions (Figs. 5b and 5d) [24, 58, 61]. This information is in agreement with the results obtained from the polarization curves.

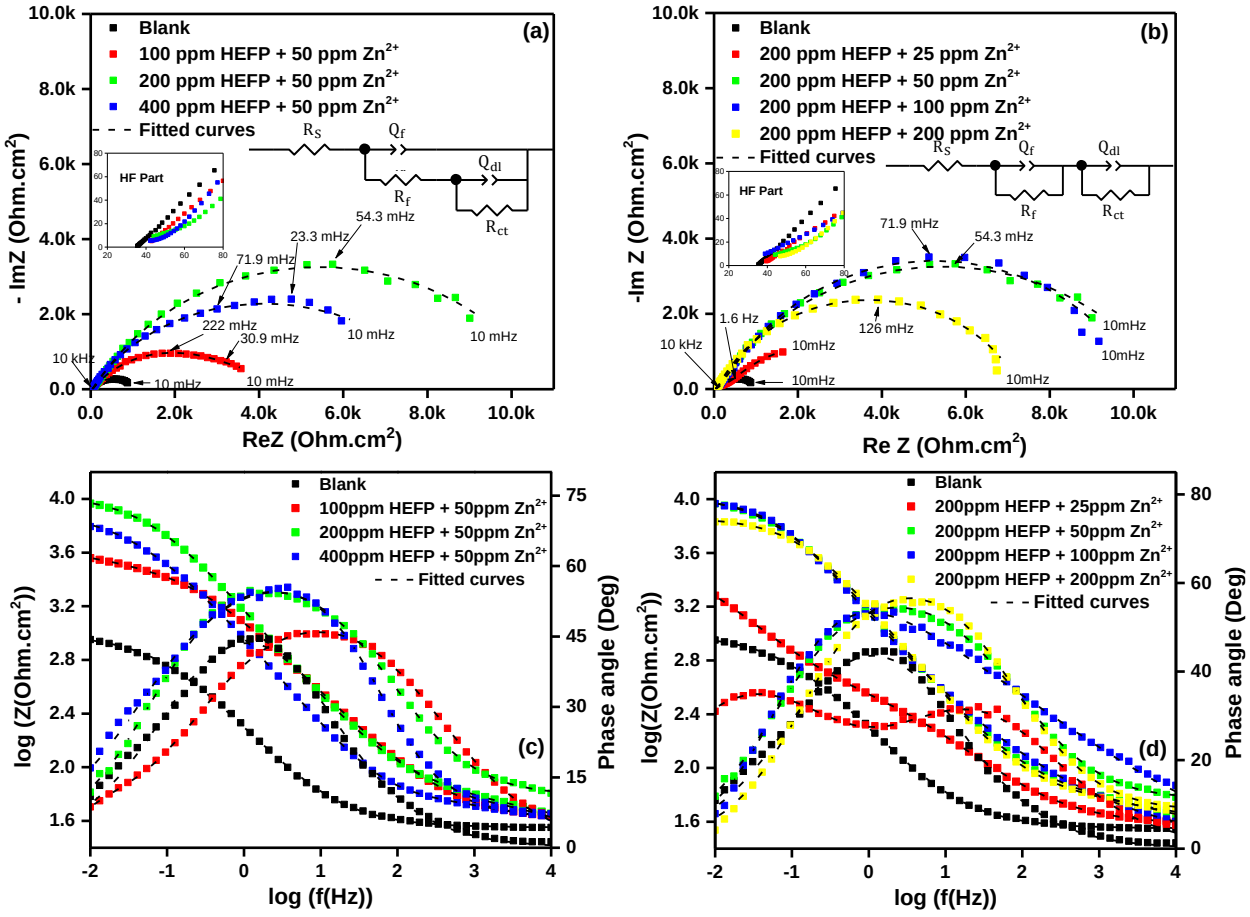

Fig. 5. Nyquist (a and b) and Bode (c and d) curves for the XC38 steel in 0,1M NaCl solution in the absence and in the presence of the HEFP + Zn^{2+} mixture.

In the presence of the mixture, except for the 200 ppm HEFP + 25 ppm Zn^{2+}, a broader peak is visible on the Bode phase diagrams. This peak is probably a combination of two time constants, one assignable to the double layer and the other to the protective film formed at high frequencies domain [24, 59]. The proximity in terms of frequency of these two time constants probably means that the protective film formed in the presence of the HEFP + Zn^{2+} mixture

adheres well to the steel surface, which is not the case when the HEFP is used as the sole inhibitor.

In the presence of 200 ppm HEFP + 25 ppm Zn^{2+}, two time constants are clearly visible on the corresponding Bode phase diagram. This observation is quite understandable. In view of the small amount of Zn^{2+} added, some organic compounds likely to chelate zinc ions are free. Poorly soluble compounds would then be formed between the excess of organic compounds and the metal cations from the iron oxidation. Since this complexation does not take place near to the metal surface, the resulting deposit will not adhere to the steel surface and therefore there will be no protection [21]. This justifies the small increase in the loop diameter observed in this case compared to the other formulations [7]. The presence of Zn^{2+} would therefore allow the diffusion and adsorption of a significant amount of the compounds present in the extract onto the steel surface. The EECs used to fit the metal/electrolyte interface in the presence of the HEFP + Zn^{2+} mixture are presented as insets in Figs 5a and 5b. These EECs were selected in line with the Bode phase diagram obtained in NaCl solution and they shows a good fitting of the experimental data (chi-square of the order of 10^{-5} and 10^{-4}) [32, 36, 58, 61]. The electrochemical data (charge transfer resistance (R_{ct}), the CPE parameters related to the electrical double layer (n_{dl} and Q_{dl}), the film resistance (R_f) and the CPE parameters related to the protective film (n_f, Q_f)) obtained from these EIS analyses are presented in Table 3. In comparison with the parameters obtained in the absence of the inhibitor, a significant increase of R_{ct} and a decrease of Q_{dl} are observed in the presence of the mixture, except in the presence of 200 ppm HEFP + 25 ppm Zn^{2+} and 400 ppm HEFP + 25 ppm Zn^{2+} formulations, where an increase of the Q_{dl} value is observed. The decrease of Q_{dl} reflects a lowering of local electricity at the metal/electrolyte interface due to the reduction of the corrosion rate by the protective layer formed on the steel surface [11]. This protective layer, which results from the synergistic action between Zn^{2+} ions and some compounds in the extract, blocks the steel oxidation sites and prevents the oxidizing agent from reaching the metal surface directly [26]. However, according to the low values of the homogeneity parameters n (n_{dl} and n_f) presented in Table 3, this layer is not uniformly distributed on the steel surface and then do not offered a perfect protection toward corrosion process. Such an observation may also justify the not very high values of the inhibition percentages obtained in the presence of the mixture.

In view of the different electrochemical results obtained, appropriate concentrations of extract and zinc ions are necessary to have an optimal synergistic effect. For all the extract

concentrations tested (100, 200 and 400 ppm), the most effective one in the formulation is 200 ppm.

Table 3. Electrochemical impedance parameters of the XC38 steel in 0.1M NaCl solution in the absence and in the presence of HEFP.

HEFP Concentration (ppm)	Zn^{2+} Concentration (ppm)	Rct (Ohm.cm^2)	n_{dl}	$Q_{dl} \times 10^{-3}$ ($\Omega^{-1}.cm^{-2}.s^{ndl}$)	Rf (Ohm.cm^2)	n_f	$Q_f \times 10^{-3}$ ($\Omega^{-1}.cm^{-2}.s^{nf}$)	Rp (Ohm.cm^2)	η_{Rct} (%)
0	0	951.9 ± 60.1	0.676 ± 0.014	1.476 ± 0.059	-	-	-	951.9 ± 60.1	-
100	25	2462.0 ± 72.7	0.526 ± 0.003	0.799 ± 0.020	1608.0 ± 67.5	0.406 ± 0.003	2.087 ± 0.240	4549.0 ± 140.2	79.1± 0.6
	50	3068.0 ± 31.8	0.625 ± 0.032	0.234 ± 0.002	1415.0 ± 16.2	0.509 ± 0.003	3.074 ± 0.040	4483.0 ± 48	78.8 ± 0.2
	100	4709.0 ± 39.1	0.655 ± 0.004	0.268 ± 0.002	99.9 ± 26.5	0.325 ± 0.071	0.260 ± 0.086	4808.9 ± 58.3	80.2 ± 0.2
	200	4044.0 ± 81.8	0.619 ± 0.117	0.197 ± 0.085	39.5 ± 5.4	0.638 ± 0.078	0.073 ± 0.014	4083.5 ± 39.1	76.7 ± 0.2
200	25	4516.0 ± 388.8	0.605 ± 0.018	2.384 ± 0.083	267.6 ± 18.8	0.592 ± 0.008	0.565 ± 0.019	4783.6 ± 407.66	80.1 ± 1.6
	50	10970.0 ± 121.2	0.679 ± 0.033	0.181 ± 0.060	37.2 ± 16.5	0.700 ± 0.192	0.032 ± 0.009	11007.2 ± 137.7	91.4 ± 0.1
	100	9092.0 ± 91.9	0.785 ± 0.004	0.211 ± 0.002	1192.0 ± 13.3	0.392 ± 0.002	0.918 ± 0.009	10284.0 ± 105.2	90.7 ± 0.1
	200	7333.0 ± 59.0	0.727 ±0.041	0.115 ± 0.055	33.3 ± 14.5	0.733 ± 0.152	0.036 ± 0.011	7366.3 ± 73.5	87.1 ± 0.1
400	25	1655.0 ± 47.8	0.662 ± 0.010	4.300 ± 0.102	266.2 ± 7.0	0.586 ± 0.003	0.738 ± 0.009	1921.2 ± 54.8	50.5 ± 1.3
	50	8414.0 ± 161.0	0.807 ± 0.017	0.106 ± 0.016	31.7 ± 2.6	0.571 ± 0.011	0.215 ± 0.016	8445.7 ± 163.6	88.7 ± 0.2
	100	8045.0 ± 82.8	0.678 ± 0.030	0.096 ± 0.031	58.4 ± 16.9	0.645 ± 0.026	0.106 ± 0.032	8103.4 ± 99.7	88.3 ± 0.1
	200	8361.0 ± 63.3	0.657 ± 0.004	0.186 ± 0.001	60.2 ± 3.0	0.662 ± 0.025	0.056 ± 0.011	8421.2 ± 66.3	88.7 ± 0.1

3.2.3 Electrochemical impedance spectroscopy around the corrosion potential

In order to provide more arguments to elucidate the inhibition mechanism of the HEFP + Zn^{2+} mixture, EIS analyses around the corrosion potential in the absence and in the presence of 200 ppm HEFP + 100 ppm Zn^{2+} were performed. These analyses should help to determine which reaction (anodic or cathodic) controls the faradic impedance response of the electrochemical system (Z_F). At corrosion potential Z_F is the component of an anodic impedance (Za) and a cathodic impedance (Zc) connected in parallel [62]. The impedance response obtained at Ecorr – 50 mV is mainly due to the cathodic impedance describing the kinetics of the reduction reaction of oxidizing agent, and the impedance response obtained at Ecorr + 50 mV is due to the anodic impedance reflected by the kinetics of steel oxidation reaction. Figure 6 show the results obtained from these analyzes in term of Nyquist and Bode diagrams. The electrochemical parameters obtained from these Nyquist curves are presented in Table 4. The EECs used to model the metal/electrolyte interface are presented as insets in Figs 6a and 6b. In the absence of inhibitor at Ecorr - 50mV a diffusion process is perceptible at low frequency on

the Nyquist curve. The EEC used to fit the EIS date obtained in this case content a diffusion-related Warburg impedance (W).

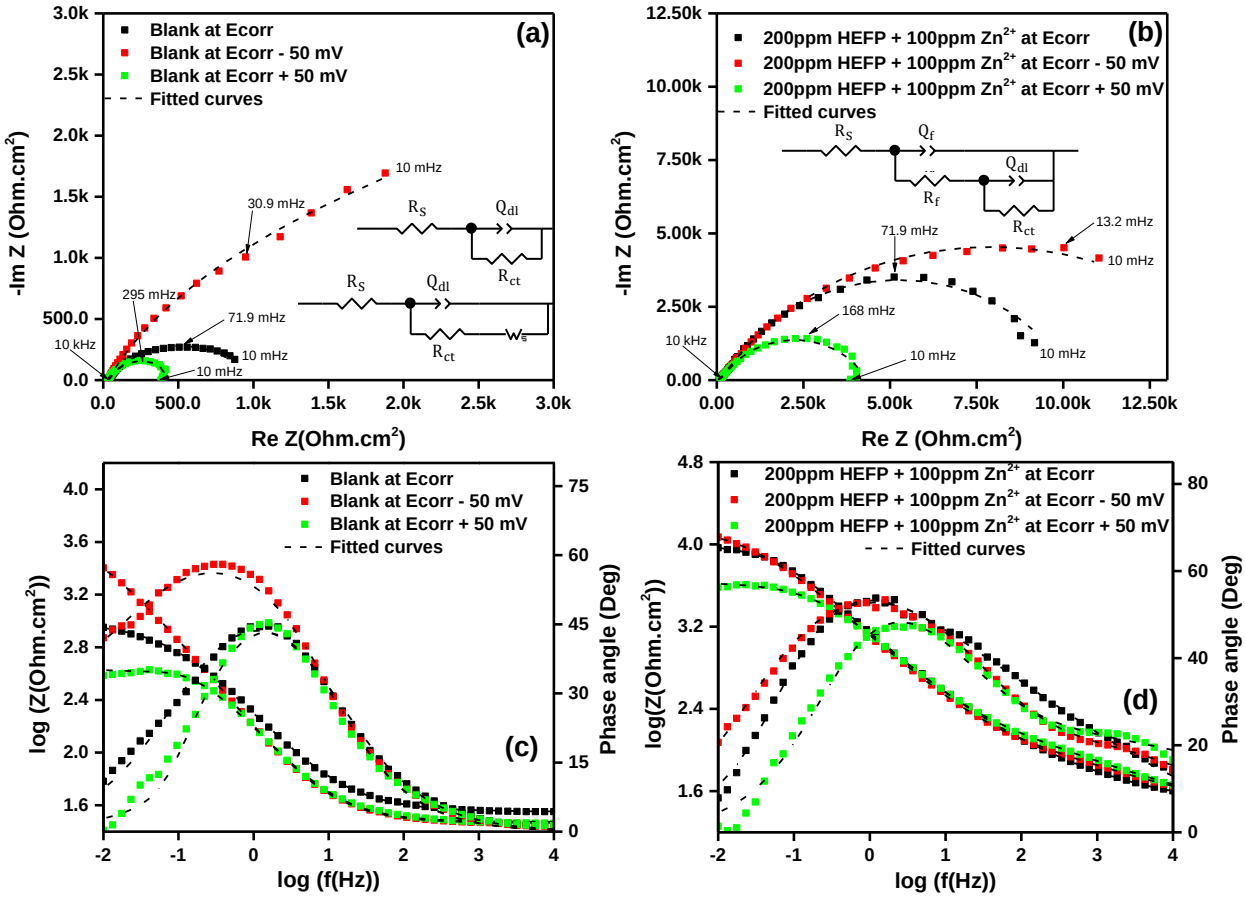

Fig. 6. Nyquist and Bode diagrams recorded around the corrosion potential of the XC38 steel in 0.1 M NaCl solution in the absence (a and c) and in the presence of 200 ppm HEFP + 100 ppm Zn^{2+} (b and d).

In the absence and in the presence of HEFP + Zn^{2+} mixture, the polarization resistance Rp, increase continuously with the potential (Rp (Ecorr + 50 mV) < Rp (Ecorr) < Rp (Ecorr + 50 mV)) meaning that Za << Zc. The impedance response of the system is therefore mainly anodic (i.e. Z_F = Za) under these experimental conditions.

The electrochemical data (charge transfer resistance (R_{ct}), the CPE parameters related to the electrical double layer (n_{dl} and Q_{dl}), the film resistance (R_f) and the CPE parameters related to the protective film (n_f, Q_f) obtained from these EIS analyses are presented in Table 4.

The inhibition percentages obtained at Ecorr and Ecorr + 50 mV in relation to Rp are very close (90.7% and 90.5% respectively) and are higher than the percentage obtained at Ecorr - 50mV in the presence of 200 ppm HEFP + 100 ppm Zn^{2+}. At Ecorr + 50 mV, the steel oxidation

reaction is favored and oxidation products are formed much faster. The equality of the inhibitory efficiencies at Ecorr and Ecorr + 50 mV further reflects the fact that the Fe(II) and Fe(III) ions produced during the steel oxidation participate in the synergistic mechanism between the organic compounds and the zinc ions. Their contributions should therefore be considered when elaborating the inhibition mechanism of the HEFP + Zn^{2+} formulations.

Table 4. Electrochemical parameters obtained from Nyquist curves of the XC38 steel in 0.1 M NaCl solution in the absence and in the presence of 200 ppm HEFP + 100 ppm Zn^{2+}.

Potential	Inhibitor Concentration	R_{ct} (Ohm.cm^2)	n_{dl}	$Q_{dl} \times 10^{-3}$ (Ω^{-1}.cm^{-2}.s^{ndl})	R_f (Ohm.cm^2)	n_f	$Q_f \times 10^{-3}$ (Ω^{-1}.cm^{-2}.s^{nf})	R_p (Ohm.cm^2)	η_{Rp} (%)
at Ecorr	Blank	951.9 ± 60.1	0.676 ± 0.014	1.476 ± 0.059	-	-	-	951.9 ± 60.1	-
	200ppm HEFP +100ppmZn^{2+}	9092.0 ± 91.9	0.785 ± 0.004	0.211 ± 0.002	1192.0 ± 13.3	0.392 ± 0.002	0.918 ± 0.009	10284.0 ± 105.2	90.7 ± 0.1
at Ecorr – 50 mV	Blank	3902.0 ± 353.2	0.715 ± 0.005	1.819 ± 0.023	-	-	-	3902.0 ± 353.2	-
	200ppm HEFP +100ppmZn^{2+}	16140.0 ± 293.6	0.660 ± 0.020	0.176 ± 0.036	80.3 ± 18.6	0.656 ± 0.078	0.049 ± 0.036	16220.3 ± 312.2	75.9 ± 0.5
at Ecorr + 50 mV	Blank	423.2 ± 8.7	0.727 ± 0.010	1.471 ± 0.046	-	-	-	423.2 ± 8.7	-
	200ppm HEFP +100ppmZn^{2+}	4334.0 ± 91.6	0.701 ± 0.33	0.144 ± 0.038	107.2 ± 32.1	0.668 ± 0.161	0.039 ± 0.014	4441.2 ± 123.7	90.5 ± 0.2

3.2.4 Surface analysis by SEM / EDX

SEM and EDX mapping images of the XC38 steel samples in 0.1 M NaCl solution after 5h of immersion in the absence of the inhibitor, in the presence of 200 ppm HEFP and 200 ppm HEFP + 100 ppm Zn^{2+} are presented in Figs 7a, 7b and 7c, respectively. In Fig. 7a (control), degradation areas are visible on the metal surface with pitting corrosion sites probably caused by chloride ions [6, 22]. It is known that aggressive anions, such as chloride, cause the breakdown of passive oxide layers present on the metal surface. The corrosion rate is usually high at these points compared to the rest of the steel surface. The EDX mapping of a steel surface in absence of the inhibitor (Fig. 7a) shows an important amount of oxygen on the surface, not uniformly distributed and attributable to the oxide layer formed. Due to its porosity, this layer offers poor protection, thus justifying the low corrosion resistance of XC38 steel in the absence of an inhibitor obtained during the electrochemical measurements. Indeed, the uncovered zones of the surface are preferential attack zones for aggressive agents.

Fig. 7b shows the topography of an area of the XC38 steel surface in the presence of 200 ppm HEFP. Localized corrosion sites are also visible as proof of a preferential adsorption of chloride ions on steel surface compared to the compounds present in the extract [5]. In contrast with the first case analyzed, a low oxygen content is observed on the EDX mapping of the steel surface. This probably means that the presence of the extract alone prevents the formation of an oxide

layer, probably because of the complexing character of its compounds, which would bind the metal cations (Fe(II) and Fe(III)) to form organometallic complexes. These complexes are not very soluble but only weakly bound to the steel surface [21]. In addition, a low proportion of Carbon element on the steel surface can be seen on the EDX spectrum in the presence of 200 ppm of HEFP (Fig. 7b). This information confirms the results obtained by linear polarization in the presence of the extract alone, in which a very low adsorption of inhibitive compounds was observed.

Fig. 7. SEM/EDX mapping of the XC38 steel surface in 0,1M NaCl solution without the inhibitor (a), and in the presence of 200 ppm HEFP (b) and 200 ppm HEFP + 100 ppm Zn^{2+} (c).

In the presence of 200 ppm HEFP + 100 ppm Zn^{2+} (Fig. 7c), the localized corrosion sites are almost non-existent on the steel surface, thus reflecting an inhibition of the pitting corrosion phenomenon following the synergistic action of the organic compounds and the Zn^{2+} ions. This pitting inhibition may be achieve by: (i) improving the protective nature of the film by changing its composition and structure; (ii) reducing the imperfections in the film; and (iii) reducing the extent of anion adsorption on the film by competitive adsorption between chloride ions and organometallic compounds [2]. The elemental mapping and EDX spectrum obtained in the presence of the HEFP + Zn^{2+} formulation reveals that Oxygen element is better distributed on the analyzed steel surface than in the two previous situations (Blank and 200 ppm HEFP). This result means that the HEFP + Zn^{2+} mixture leads to the formation of a protective layer on the steel surface probably consisting of oxide layers and adsorbed organometallic compounds. The pitting corrosion inhibition mechanism (i) and (ii) are then possible in this experimental condition. The presence of carbon on the EDX spectrum in a higher proportion (relative to Iron element) than those obtained in the absence of inhibitor and in the presence of 200 ppm of HEFP also confirms these possibilities. Zinc-covered areas are also highlighted on the elemental maps shown in Fig. 7c. This zinc layer correspond to zinc oxy-hydroxides formed preferentially at cathodic sites by reaction between Zn^{2+} ions and OH^- ions [24, 26].

In view of the results obtained from these surface analyses, the presence of Zn^{2+} ions would therefore facilitate the diffusion and quantitative adsorption of the organic compounds on the metal surface, thus justifying the good inhibitive efficiency observed in the presence of HEFP + Zn^{2+} formulations.

4. Mechanism of corrosion inhibition by the plant extract + Zn^{2+} formulation: simulation of the synergistic effect

The synergistic effect mechanism between the HEFP and the zinc ions has been proposed based on the experimental results described above. In order to facilitate the mechanism presentation, the corrosion process of steel in NaCl medium should be recalled. When the steel is immersed in an aerated NaCl solution in the absence of an inhibitor, there are two principal reactions which control the anodic and the cathodic response in terms of the faradic current. The cathodic reaction is mainly the reduction of dissolved oxygen (4) and the anodic reaction is the oxidation of Fe(0) to ferrous ions (5). Ferrous ions in solution can oxidize to ferric ions (6) [63, 64].

$$O_2 + 2H_2O + 4e^- \leftrightarrow 4OH^- \quad (4)$$

$$Fe \leftrightarrow Fe^{2+} + 2e^- \quad (5)$$

$$Fe^{2+} \leftrightarrow Fe^{3+} + e^- \quad (6)$$

According to the electrochemical results described above, the inhibitive activity observed between the HEFP and Zn^{2+} ions is mainly due to the reactivity at the interface of organometallic complexes formed between Zn^{2+} and some compounds present in the extract. This is in line with some reports described in the literature [25, 26, 32, 33, 35, 36, 61]. However, the contribution of steel oxidation products (Fe(II) and Fe(III) ions) should be considered in the synergistic process, since these ions are present at the metal-electrolyte interface and some extract inhibitive compounds (as polyphenols) can chelate them forming more stable complexes than with Zn^{2+} ions [32, 37, 39]. A concerted mechanism between the zinc ions, the steel oxidation products and the extract compounds able to chelate Iron(II) and Iron(III) is then possible and would justify the inhibitive efficiency observed in the presence of the HEFP + Zn^{2+} formulations. One interesting approach to clarify this issue is to evaluate the electrochemical behavior of steel in the presence of formulations based on Zn^{2+} and some active inhibitor compounds contained in the extracts.

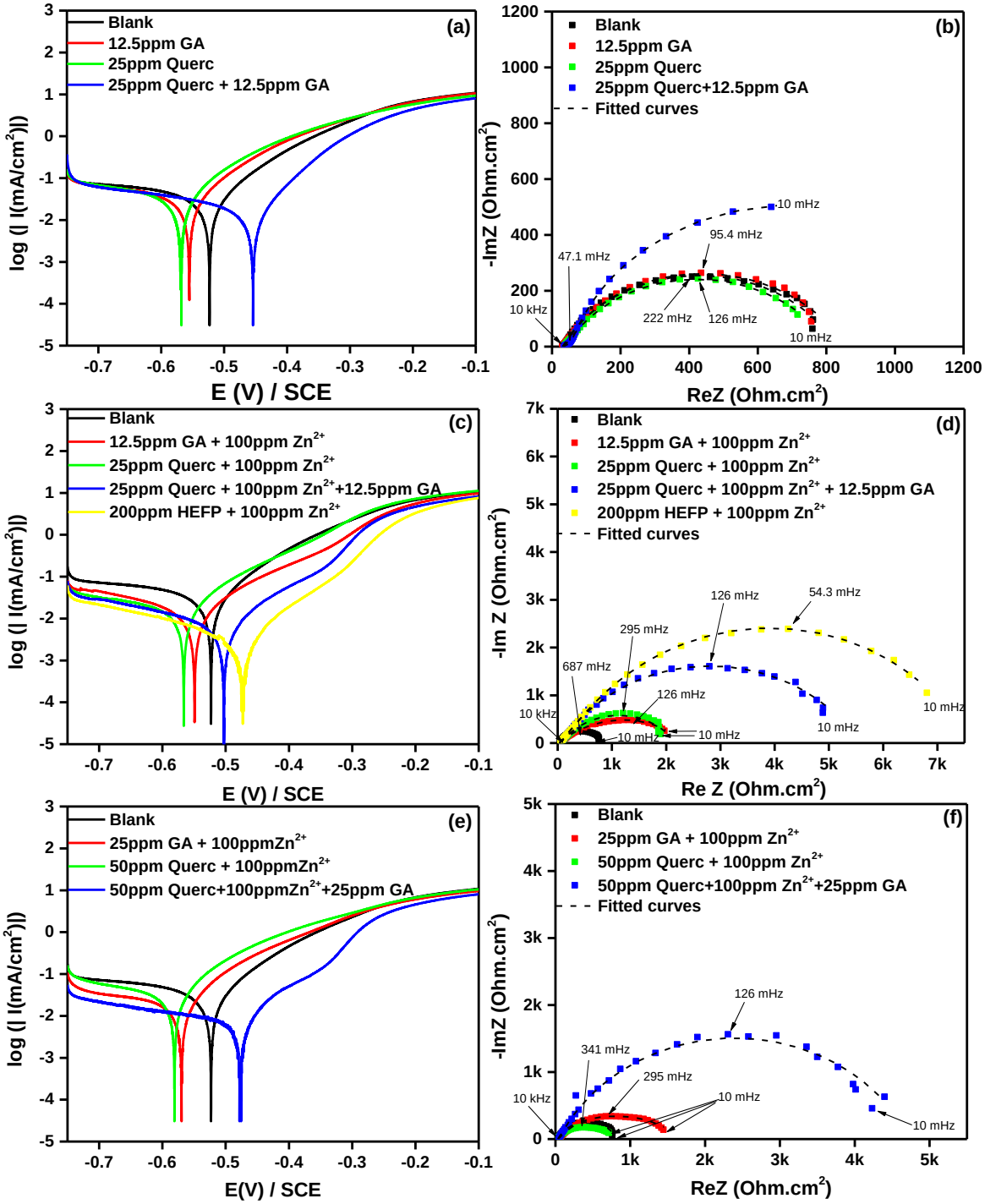

Fig. 8. Polarization (a, c and e) and Nyquist (b, c and f) curves of the XC38 steel in 0,1M NaCl in the presence of GA, Querc, GA + Zn^{2+}, Querc + Zn^{2+}, Querc + GA + Zn^{2+} and HEFP + Zn^{2+}.

Phytochemical tests revealed the presence of phenolic compounds and flavonoids in the extract. It is known that flavonoids with a keto group and an adjacent hydroxyl group bonded to carbons in the 3–4 or 4–5 positions form stable complexes with Fe(II), while compounds with catechol and galloyl groups (such as phenolic acids) form very stable complexes with Fe(III). An electrochemical evaluation of the corrosion inhibitive efficiency of a mixture of flavonoid

(quercetin), phenolic acid (gallic acid) and zinc ions would allow to validate the concerted mechanism proposed. Quercetin will serve as the main Iron(II) chelating agent and gallic acid as the Iron(III) chelating agent. The chemical structures of quercetin and gallic acid are presented in Supplementary Information. The flavonoid concentrations used (25ppm and 50ppm) are close to that evaluated in the plant extract (26.7 ppm of total flavonoids for 200 ppm of extract) in order to reproduce the conditions of the inhibitive behavior observed with the HEFP + Zn^{2+} formulation. The polarization and Nyquist curves of the XC38 steel obtained in the presence of quercetin (Querc), gallic acid (GA), Querc + GA and Querc+GA+Zn^{2+} formulations are shown in Fig. 8.

For these experiments, the electrolytic solution (0.1 M NaCl) was adjusted to pH 10 with a few drops of a molar solution of NaOH in order to solubilize quercetin. For comparison, the results obtained with the 200ppm HEFP + 100ppm Zn^{2+} formulation are also presented. The electrochemical parameters obtained from the polarization and Nyquist curves are presented in Tables 5 and 6, respectively.

Table 5. Kinetic parameters obtained from polarization curves of the XC38 steel in 0.1M NaCl solution in the absence and in the presence of inhibitor formulations.

Concentration	**Ecorr (mV/ECS)**	**Icorr (µA.cm^{-2})**	**β_a (mV/dec)**	**-β_c (mV/dec)**	**Rp (Ohm.cm^2)**	**η_{Icorr} (%)**	**η_{Rp} (%)**
Blank	-524 ± 9	32.3 ± 1.4	108.4 ± 2.2	454.7 ± 26.9	923 ± 77	-	-
12.5ppm GA	-557 ± 6	34.2 ± 0.8	111.1 ± 7.4	515.6 ± 25.3	831 ± 38	-	-
25ppm Querc	-570 ± 14	34.4 ± 3.9	107.3 ± 15.2	443.7 ± 79.8	827 ± 156	-	-
25ppm Querc + 12.5ppm GA	-456 ± 11	18.8 ± 0.7	87.4 ± 3.6	458.8 ± 15.4	1563 ± 53	41.8 ± 2.2	40.9 ± 2.0
25ppm Querc + 100ppm Zn^{2+}	-568 ± 2	16.5 ± 0.6	110.0 ± 8.3	458.4 ± 3.4	1601 ± 137	48.9 ± 1.8	42.3 ± 4.6
12.5ppm GA + 100ppm Zn^{2+}	-584 ± 16	14.3 ± 0.5	129.8 ± 10.6	300.9 ± 47.3	2054 ± 271	55.7 ± 1.6	55.1 ± 4.6
25ppm GA + 100ppm Zn^{2+}	-625 ± 17	19.4 ± 1.2	143.1 ± 5.7	268.1 ± 15.4	1408 ± 94	39.9 ± 3.7	34.4 ± 4.1
50ppm Querc + 100ppm Zn^{2+}	-583 ± 10	34.0 ± 1.1	144.2 ± 6.2	330.8 ± 12.4	793 ± 25	-	-
25ppm Querc + 100ppmZn^{2+} + 12.5ppm GA	-536 ± 8	6.3 ± 0.5	107.7 ± 2.3	290.0 ± 34.4	6014 ± 41	77.4 ± 4.6	76.9 ± 7.9
50ppm Querc +100ppm Zn^{2+} + 25ppm GA	-478 ± 1	6.9 ± 0.7	104.1 ± 12.4	547.3± 41.8	3166 ± 186	75.9 ± 4.9	70.8 ± 1.7
200ppm HEFP + 100ppm Zn^{2+}	-475 ± 8	3.6 ± 0.2	101.0 ± 8.9	284.3 ± 17.3	8844 ± 66	88.9 ± 0.6	89.6 ± 0.1

Used as the sole inhibitor, GA and Querc are not effective against corrosion of the XC38 steel in NaCl solution, as shown in Figs 8a and 8b. However, in the presence of a mixture of GA and Querc, the corresponding polarization and EIS curves show a very slight decrease of the anodic current and a small increase in the diameter of the Nyquist loop compared to the control (blank). In addition, the shapes of these curves are very similar to those obtained when the plant

extract was used as the only inhibitor (Fig 3). This result probably means that, under these conditions, the Querc + GA mixture acts through the same mechanism as the extract, i.e. by the formation of poorly soluble organometallic compounds that do not perfectly adhere to the metal surface.

Table 6. Electrochemical impedance parameters obtained from Nyquist curves of the XC38 steel in 0.1M NaCl solution in the absence and in the presence of inhibitor formulations.

Concentration	**R_{ct} (Ohm.cm^2)**	**n_{dl}**	**$Q_{dl} \times 10^{-3}$ (Ω^{-1}.cm^{-2}.s^{ndl})**	**R_f (Ohm.cm^2)**	**n_f**	**$Q_f \times 10^{-3}$ (Ω^{-1}.cm^{-2}.s^{nf})**	**Rp (Ohm.cm^2)**	**η_{Rp} (%)**
Blank	796.3 ± 7.8	0.725 ± 0.004	1.076 ± 0.013	-	-	-	796.3 ± 7.8	-
12.5ppm GA	709.4 ± 32.5	0.701 ± 0.005	1.331 ± 0.06	113.8 ± 35.3	0.921 ± 0.071	0.189 ± 0.06	823.2 ± 67.8	-
25ppm Querc	661.8 ± 40.2	0.695 ± 0.012	1.511 ± 0.146	113.2 ± 44.6	0.792 ± 0.070	0.404 ± 0.142	775.0 ± 84.8	-
25ppm Querc + 12.5ppm GA	1510.0 ± 105.9	0.849 ± 0.030	6.159 ± 0.069	23.5 ± 3.6	0.677 ± 0.049	2.097 ± 0.638	1533.5 ± 102.3	48.1 ± 3.2
25ppm Querc + 100ppm Zn^{2+}	2122.0 ± 33.9	0.630 ± 0.023	0.260 ± 0.066	39.3 ± 19.6	0.660 ± 0.530	0.026 ± 0.019	2161.3 ± 53.5	63.2 ± 0.8
12.5ppm GA + 100ppm Zn^{2+}	1802.0 ± 113.0	0.535 ± 0.062	0.625 ±0.191	492.6 ± 75.4	0.511 ± 0.030	0.757 ± 0.258	2294.6 ± 188.4	65.3 ± 2.6
25ppm GA + 100ppm Zn^{2+}	1399.0± 68.0	0.513 ± 0.011	0.724 ± 0.142	238.0 ± 87.1	0.793 ± 0.057	0.733 ± 0.078	1637.0 ± 155.1	51.4 ± 4.2
50ppm Querc + 100ppm Zn^{2+}	532.9 ± 27.9	0.592 ± 0.006	0.282 ± 0.033	246.1 ± 28.9	0.749 ± 0.016	1.033 ± 0.034	779.0 ± 56.8	-
25ppmQuerc + 100ppm Zn^{2+} + 12.5ppm GA	5365.0 ± 39.0	0.692 ± 0.003	0.218 ± 0.048	66.2 ± 8.3	0.506± 0.025	0.614± 0.117	5431.2 ± 47.3	85.3 ± 0.2
50ppm Querc +100ppm Zn^{2+} +25ppm GA	4703.0 ± 75.3	0.721 ± 0.140	0.213± 0.007	11.2 ± 0.8	0.747 ± 0.003	0.061 ± 0.005	4714.2 ± 76.1	83.1 ± 0.3
200ppm HEFP + 100ppm Zn^{2+}	6695 ± 630	0.756 ± 0.040	0.294 ± 0.091	853.3 ± 337.6	0.546 ± 0.073	0.920 ± 0.211	7548.3 ± 967.6	89.5 ± 1.1

In the presence of the Querc + GA + Zn^{2+} formulations, the polarization curves (Figs. 8c and 8e) show a similar trend to that observed in the presence of 200ppm HEFP + 100ppm Zn^{2+} (Fig. 8c). Smaller cathodic and anodic currents are recorded in both cases and a desorption phenomenon is observed on the anodic branches between -0.35 and -0.25V/ECS. In comparison with the results obtained in the presence of GA + Zn^{2+} and of Querc + Zn^{2+}, the inhibition percentages (related to Icorr and to Rp) increase considerably when the Querc + GA + Zn^{2+} formulation is used. This proves that the amount of organic compounds adsorbed on the steel surface in the latter case is more important and the film formed is therefore more protective. The Nyquist diagrams obtained (Figs. 8d and 8f) confirm these results. A considerable increase of the capacitive loop diameter is observed in the presence of the Querc + GA + Zn^{2+} formulations showing a much higher steel corrosion resistance in this case compare to the results obtained in the presence of GA + Zn^{2+} and of Querc + Zn^{2+}. These observations prove that by combining quercetin and gallic acid in the presence of Zn(II) ions, the inhibitive activity of the formulation is considerably improved. Knowing that quercetin is

an Iron(II) chelating agent and gallic acid has a good affinity with Iron(III), the synergistic mechanism proposed above, is therefore possible. This inhibition mechanism, as described in Fig 9, suggests a concerted action between quercetin, gallic acid, steel oxidation products (Fe^{2+} and Fe^{3+}) and zinc ions when using the Querc + GA + Zn^{2+} formulations for corrosion inhibition of the XC38 steel in 0.1M NaCl solution. The result of this concerted action is the formation on the steel surface of a protective layer composed of corrosion products, $Zn(OH)_2$ and adsorbed organometallic complexes. The low values of the homogeneity parameters ndl and nf (Table 6) prove that this layer is not uniformly distributed on the steel surface, which could also justify the fact that the inhibition percentages are not very high.

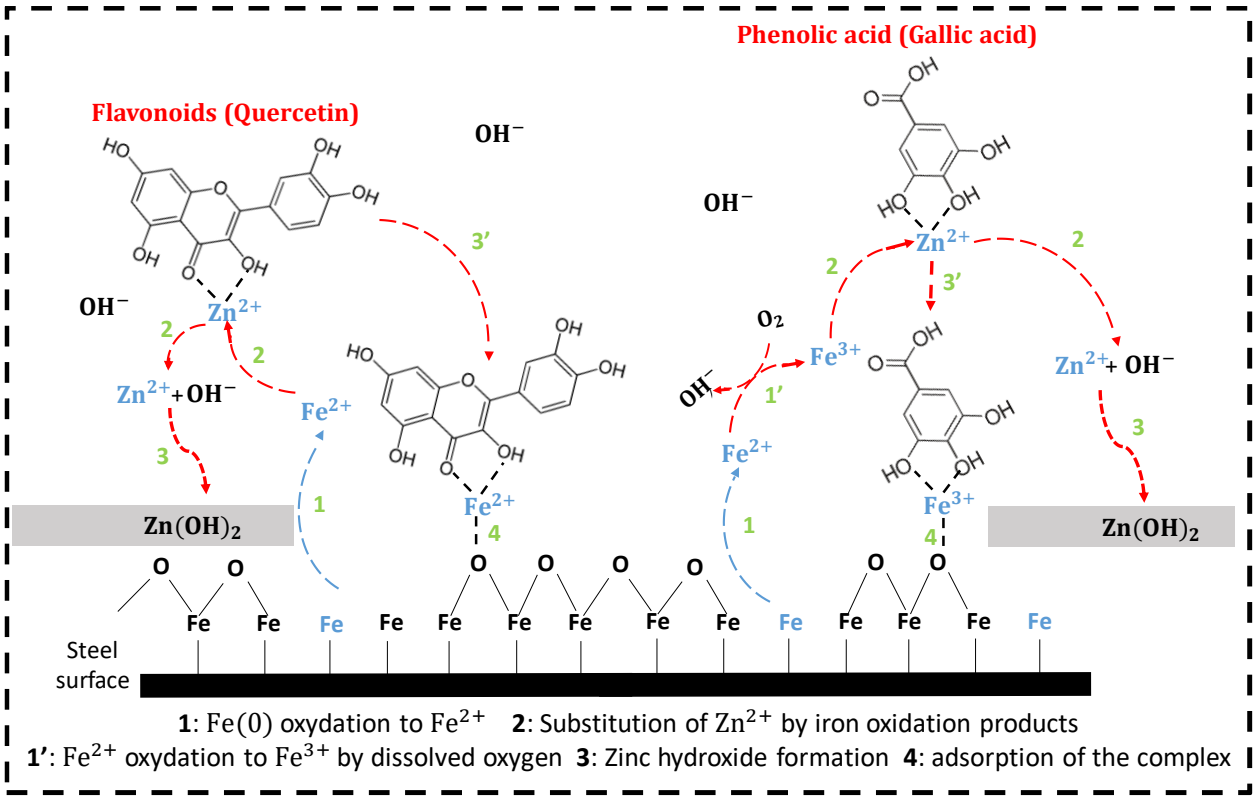

Fig. 9. Inhibition mechanism proposed when a mixture of flavonoid, phenolic acid and zinc ions are used for corrosion inhibition of steel in NaCl solution.

Further analysis of Table 6 reveals that, some of the electrochemical parameters (as tafel slopes β_a and $-\beta_c$, and CPE parameters related to the double layer) and the inhibition percentages obtained in the presence of the Querc + GA + Zn^{2+} formulations are not far from those obtained in the presence of 200ppm HEFP + 100ppm Zn^{2+}. Such results suggest a possible mechanistic similarity between the inhibitive activities of the Querc + GA + Zn^{2+} mixture and the HEFP + Zn^{2+} formulation when used as steel corrosion inhibitors in NaCl medium. According to Fig. 9, the inhibition mechanism proposed for the HEFP + Zn^{2+} formulations can now be described

in four steps : (i) Quantitative diffusion of organometallic complexes to the steel surface, due to their high solubility. (ii) Substitution of chelated Zinc(II) ions by Fe(II) or Fe(III) ions present at the metal/electrolyte interface, due to the stability criteria [32, 37, 39]. (iii) Adsorption of new complexes, formed in a very close area of the steel surface, leading to the formation of a protective film. (iv) Chemical reaction between the released Zn^{2+} ions and the OH^- ions from oxygen reduction to form a $Zn(OH)_2$ deposit on the steel surface, which reinforces the protective capacities of the film.

5. Conclusion

The inhibitive activity and the inhibitor concentration effect of a mixture of zinc salt and *Ficus pumila leaves* hydroalcoholic extracts against corrosion of the XC38 steel in NaCl solution were investigated. Electrochemical measurements coupled with surface characterizations by SEM/EDX analysis proved that the presence of zinc ions significantly increases the inhibiting capacity of the HEFP against steel corrosion. Based on the electrochemical results obtained, appropriate concentrations of zinc ions and plant extract are needed to have an optimal inhibitive capacity. The highest inhibition percentages (91.3% and 88.9%) were obtained with the 200 ppm HEFP + 50 ppm Zn^{2+} and 200 ppm HEFP + 100 ppm Zn^{2+} formulations, respectively, while the 200 ppm HEFP, 50 ppm Zn^{2+} and 100 ppm Zn^{2+} each provided inhibition percentages of 39.9%, 3.3% and –6.3%, respectively. The high inhibitive activity of these formulations is mainly due to the reactivity at the metal/electrolyte interface of the organometallic complexes formed between zinc ions and some compounds present in the extract, like polyphenols, which facilitate the formation of a very protective film on the steel surface. An inhibition mechanism is proposed according to the results obtained when a formulation of flavonoid (quercetin), phenolic acid (gallic acid) and zinc ions is used for corrosion inhibition, since these organic compounds are susceptible to be present in the extract and are able to form complexes with metal cations. A concerted mechanism between zinc ions, steel oxidation products (Iron(II) and Iron(III)) and complexing agents contained in the HEFP would be responsible of the inhibitive efficiency observed when the HEFP + Zn^{2+} formulations are used to inhibit corrosion of the XC38 steel in NaCl solution.

Acknowledgements

The authors acknowledge the support of the Agence Universitaire de la Francophonie through the grant AUF-DRACGL-2017-006, the ISP through the grant offered to the African Network

of Electroanalytical Chemists (ANEC), the Centre National de la Recherche Scientifique (CNRS) and the Université Paris-Saclay.

References

1. P.A. Schweitzer, Fundamentals of corrosion : Mechanisms, Causes, and Preventative Methods, CRC press, Boca Raton, 2010.
2. V.S. Sastri, Green corrosion inhibitors: theory and practice, John Wiley & Sons, New Jersey, 2012.
3. L. Cáceres, T. Vargas, L. Herrera, Influence of pitting and iron oxide formation during corrosion of carbon steel in unbuffered NaCl solutions, Corros. Sci. 51 (2009) 971–978. https://doi.org/10.1016/j.corsci.2009.02.021.
4. Y.F. Cheng, M. Wilmott, J.L. Luo, The role of chloride ions in pitting of carbon steel studied by the statistical analysis of electrochemical noise, Appl. Surf. Sci. 152 (1999) 161–168. https://doi.org/10.1016/S0169-4332(99)00328-1.
5. O.R. Wamba Tchio, M. Pengou, C. Baumier, S. Franger, A.L. Teillout, I. M. Mbomekallé, P. De Oliveira, C. P. Nanseu-Njiki, E. Ngameni, Comparison between Lacunary and Saturated Keggin Polyoxometalates as Steel Corrosion Inhibitors in Chloride Solution: Contribution of the Lacuna the Inhibition Mechanism. ChemistrySelect, 5 (2020) 10135–10143. https://doi.org/10.1002/slct.202001591.
6. B. Baroux, La corrosion des metaux: Passivite et corrosion localisee, Dunod, Grenoble, 2014.
7. Y.I. Kuznetsov, A.D. Mercer, J.G.N. Thomas, Organic Inhibitors for Corrosion of Metals, Plenum Press, New York, 1996.
8. A. Dehghani, G. Bahlakeh, B. Ramezanzadeh, A.H. Mostafatabar, M. Ramezanzadeh, 2020. Estimating the synergistic corrosion inhibition potency of (2-(3,4-)-3,5,7-trihydroxy-4H-chromen-4-one) and trivalent-cerium ions on mild steel in NaCl solution. Constr. Build. Mater. 261, 119923. https://10.1016/j.conbuildmat.2020.119923.
9. G.K. Shamnamol, J.M. Jacob, P. Rugma, J.R. Anoop Raj, Synergistic effect of salts on the corrosion inhibitive action of plant extract: a review, J. Adhes. Sci. Technol. 35 (2021) 133–163. https://doi.org/10.1080/01694243.2020.1797336.
10. B. Matangouo, G.K. Dedzo, L. Dzene, C.P. Nanseu-Njiki, E. Ngameni, 2021. Encapsulation of butylimidazole in smectite and slow release for enhanced copper

corrosion inhibition. Appl. Clay Sci. 213, 106266. https://doi.org/10.1016/j.clay.2021.106266.

11. B. Ngouné, M. Pengou, A.M. Nouteza, C.P. Nanseu-Njiki, E. Ngameni, Performances of alkaloid extract from Rauvolfia macrophylla Stapf toward corrosion inhibition of C38 steel in acidic media, ACS omega, 4 (2019) 9081–9091. https://doi.org/10.1021/acsomega.9b01076.
12. A. Dehghani, A.H. Mostafatabar, G. Bahlakeh, B. Ramezanzadeh, 2020. A detailed study on the synergistic corrosion inhibition impact of the Quercetin molecules and trivalent europium salt on mild steel; electrochemical/surface studies, DFT modeling, and MC/MD computer simulation. J. Mol. Liq. 316, 113914. https://doi.org/10.1016/j.molliq.2020.113914.
13. M. Jokar, T.S. Farahani, B. Ramezanzadeh, Electrochemical and surface characterizations of morus alba pendula leaves extract (MAPLE) as a green corrosion inhibitor for steel in 1 M HCl, J. Taiwan Inst. Chem. Eng. 63 (2016) 436–452. https://doi.org/10.1016/j.jtice.2016.02.027.
14. K. Anupama, K. Shainy, A. Joseph, 2016. Excellent anticorrosion behavior of Ruta Graveolens extract (RGE) for mild steel in hydrochloric acid: electro analytical studies on the effect of time, temperature, and inhibitor concentration. J. Bio Tribo Corros. 2, 2. https://doi.org/10.1007/s40735-016-0032-5.
15. S. Martinez, I. Štern, Inhibitory mechanism of low-carbon steel corrosion by mimosa tannin in sulphuric acid solutions, J. Appl. Electrochem. 31 (2001) 973–978. https://doi.org/ 10.1023/A:1017989510605.
16. Y. Fang, B. Suganthan, R.P. Ramasamy, Electrochemical characterization of aromatic corrosion inhibitors from plant extracts, J. Electroanal. Chem. 840 (2019) 74–83. https://doi.org/10.1016/j.jelechem.2019.03.052.
17. A.E. Fazary, M. Taha, Y.H. Ju, Iron complexation studies of gallic acid, J. Chem. Eng. Data, 54 (2009) 35–42. https://doi.org/10.1021/je800441u.
18. Z. Fu, R. Chen, 2019. Study of complexes of tannic acid with Fe(III) and Fe(II), J. Anal. Methods Chem. 2019, 3894571. https://doi.org/10.1155/2019/3894571.
19. M. Satterfield, J.S. Brodbelt, Enhanced detection of flavonoids by metal complexation and electrospray ionization mass spectrometry, Anal. Chem. 72 (2000) 5898–5906. https://doi.org/ 10.1021/ac0007985.
20. R.S. Peres, E. Cassel, D.S. Azambuja, Black wattle tannin as steel corrosion inhibitor, Int. Scholarly Res. Not., 2012 (2012) 1–9. https://doi.org/ 10.5402/2012/937920.

21. W. Xu, E.H. Han, Z. Wang, Effect of tannic acid on corrosion behavior of carbon steel in NaCl solution, J. Mater. Sci. Technol. 35 (2019) 64–75. https://doi.org/10.1016/j.jmst.2018.09.001.
22. L. Valek, S. Martinez, D. Mikulić, I. Brnardić, The inhibition activity of ascorbic acid towards corrosion of steel in alkaline media containing chloride ions, Corros. Sci. 50 (2008), 2705–2709. https://doi.org/10.1016/j.corsci.2008.06.018.
23. A.A. Rahim, E. Rocca, J. Steinmetz, M. Kassim, R. Adnan, M.S. Ibrahim, Mangrove tannins and their flavanoid monomers as alternative steel corrosion inhibitors in acidic medium, Corros. Sci. 49 (2007) 402–417. https://doi.org/10.1016/j.corsci.2006.04.013.
24. Z. Sanaei, T. Shahrabi, B. Ramezanzadeh, Synthesis and characterization of an effective green corrosion inhibitive hybrid pigment based on zinc acetate-Cichorium intybus L leaves extract (ZnA-CIL. L): Electrochemical investigations on the synergistic corrosion inhibition of mild steel in aqueous chloride solutions, Dyes Pigm. 139 (2017) 218–232. https://doi.org/10.1016/j.dyepig.2016.12.002.
25. E. Salehi, R. Naderi, B. Ramezanzadeh, Synthesis and characterization of an effective organic/inorganic hybrid green corrosion inhibitive complex based on zinc acetate/Urtica Dioica, Appl. Surf. Sci. 396 (2017) 1499–1514. https://doi.org/10.1016/j.apsusc.2016.11.198.
26. M. Ramezanzadeh, G. Bahlakeh, B. Ramezanzadeh, 2019. Study of the synergistic effect of Mangifera indica leaves extract and zinc ions on the mild steel corrosion inhibition in simulated seawater: computational and electrochemical studies. J. Mol. Liq. 292, 111387. https://doi.org/10.1016/j.molliq.2019.111387.
27. G. Bahlakeh, M. Ramezanzadeh, B. Ramezanzadeh, Experimental and theoretical studies of the synergistic inhibition effects between the plant leaves extract (PLE) and zinc salt (ZS) in corrosion control of carbon steel in chloride solution, J. Mol. Liq. 248 (2017) 854–870. https://doi.org/10.1016/j.molliq.2017.10.120.
28. K. Rajam, S. Rajendran, R. Saranya, 2013. Allium sativum (Garlic) extract as nontoxic corrosion inhibitor. J. Chem. 2013, 743807. https://doi.org/10.1155/2013/743807.
29. K. Anuradha, R. Vimala, B. Narayanasamy, J. Arockia Selvi, S. Rajendran. Corrosion inhibition of carbon steel in low chloride media by an aqueous extract of Hibiscus rosa-sinensis Linn, Chem. Eng. Commun. 195 (2007) 352–366. https://doi.org/10.1080/00986440701673283.
30. V. Johnsirani, J. Sathiyabama, S. Rajendran, S. Christyc, J. Jeyasundari, The Effect of Eclipta Alba Leaves Extract on the Corrosion Inhibition Process of Carbon Steel in Sea

Water, Port. Electrochim. Acta, 31 (2013) 95–106. https://doi.org/10.4152/pea.201302095.

31. L. Kaghazchi, R. Naderi, B. Ramezanzadeh, 2021. Synergistic mild steel corrosion mitigation in sodium chloride-containing solution utilizing various mixtures of phytic acid molecules and Zn2+ ions. J. Mol. Liq. 323, 114589. https://doi.org/10.1016/j.molliq.2020.114589.
32. M.T. Majd, M. Ramezanzadeh, B. Ramezanzadeh, G. Bahlakeh, 2020. Production of an environmentally stable anti-corrosion fi lm based on Esfand seed extract molecules-metal cations: Integrated experimental and computer modeling approaches. J. Hazard. Mater. 382, 121029. https://doi.org/10.1016/j.jhazmat.2019.121029.
33. M.T. Majd, G. Bahlakeh, A. Dehghani, B. Ramezanzadeh, M. Ramezanzadeh, 2019. Combined molecular simulation, DFT computation and electrochemical studies of the mild steel corrosion protection against NaCl solution using aqueous Eucalyptus leaves extract molecules linked with zinc ions. J. Mol. Liq. 294, 111550. https://doi.org/10.1016/j.molliq.2019.111550.
34. S. Akbarzadeh, B. Ramezanzadeh, G. Bahlakeh, M. Ramezanzadeh, 2019. Molecular/elec tronic/atomic-level simulation and experimental exploration of the corrosion inhibiting molecules attraction at the steel/chloride-containing solution interface. J. Mol. Liq. 296, 111809. https://doi.org/10.1016/j.molliq.2019.111809.
35. M.T. Majd, G. Bahlakeh, A. Dehghani, B. Ramezanzadeh, M. Ramezanzadeh, 2019. A green complex film based on the extract of Persian Echium amoenum and zinc nitrate for mild steel protection in saline solution ; Electrochemical and surface explorations besides dynamic simulation. J. Mol. Liq. 291, 111281. https://doi.org/10.1016/j.molliq.2019.111281.
36. M.T. Majd, S. Akbarzadeh, M. Ramezanzadeh, G. Bahlakeh, B. Ramezanzadeh, 2019. A detailed investigation of the chloride-induced corrosion of mild steel in the presence of combined green organic molecules of Primrose flower and zinc cations. J. Mol. Liq. 297, 111862. https://doi.org/10.1016/j.molliq.2019.111862.
37. N. Asadi, M. Ramezanzadeh, G. Bahlakeh, B. Ramezanzadeh, 2020. Theoretical MD/DFT computer explorations and surface-electrochemical investigations of the zinc/iron metal cations interactions with highly active molecules from Lemon balm extract toward the steel corrosion retardation in saline solution. J. Mol. Liq. 310, 113220. https://doi.org/10.1016/j.molliq.2020.113220.

38. M. Leopoldini, N. Russo, S. Chiodo, M. Toscano, Iron chelation by the powerful antioxidant flavonoid quercetin, J. Agric. Food Chem. 54 (2006) 6343–6351. https://doi.org/10.1021/jf060986h.
39. Y. Liu, M. Guo, Studies on transition metal-quercetin complexes using electrospray ionization tandem mass spectrometry, Molecules, 20 (2015) 8583–8594. https://doi.org/10.3390/molecules20058583.
40. J. Kaur, Pharmacognostical and Preliminary Phytochemical Studies on the Leaf Extract of Ficus pumila Linn. J. Pharmacogn. Phytochem. 1 (2012) 105–111.
41. J. Kitajima, K. Kimizuka, M. Arai, Y. Tanaka, Constituents of Ficus pumila leaves, Chem. Pharm. Bull. 46 (1998) 1647–1649. https://doi.org/10.1248/cpb.46.1647.
42. N.M Noronha, G.E. Ribeiro, I.S. Ribeiro, M.E. Marques, L.L. Coelho, J.K. Chavasco, Phytochemical profile and antioxidant and antimicrobial activities of hydroethanolic extracts of Ficus pumila, Afr. J. Microbiol. Res. 8 (2014) 2665–2671. https://doi.org/10.5897/ajmr2014.6762.
43. Q. Liu, Z. Song, H. Han, S. Donkor, L. Jiang, W. Wang, H. Chu, 2020. A novel green reinforcement corrosion inhibitor extracted from waste Platanus acerifolia leaves. Constr. Build. Mater. 260 (2020) 119695. https://doi.org/10.1016/j.conbuildmat.2020.119695.
44. M. Deyab, Inhibition activity of Seaweed extract for mild carbon steel corrosion in saline formation water, Desalination, 384 (2016) 60–67. https://doi.org/10.1016/j.desal.2016.02.001.
45. N.D. Nam, P.T.N. Ha, H.T. Anh, N.T. Hoai, P.V. Hien, Role of hydroxyl group in cerium hydroxycinnamate on corrosion inhibition of mild steel in 0.6 M NaCl solution, J. Saudi Chem. Soc. 23 (2019) 30–42. https://doi.org/10.1016/j.jscs.2018.03.005.
46. M. Abdallah, A.Y. El-Etre, M.G. Soliman, E.M. Mabrouk, Some organic and inorganic compounds as inhibitors for carbon steel corrosion in 3.5% NaCl solution, Anti-Corros. Methods Mater. 53 (2006) 118–123. https://doi.org/10.1108/00035590610650820.
47. E.B. Caldona, M. Zhang, G. Liang, T.K. Hollis, C.E. Webster, D.W., Smith Jr, D.O. Wipf, 2021. Corrosion inhibition of mild steel in acidic medium by simple azole-based aromatic compounds. J. Electroanal. Chem. 880, 114858. https://doi.org/10.1016/j.jelechem.2020.114858.
48. C. Rahal, M. Masmoudi, R. Abdelhedi, R. Sabot, M. Jeannin, M. Bouaziz, P. Refait, Olive leaf extract as natural corrosion inhibitor for pure copper in 0.5 M NaCl solution:

A study by voltammetry around OCP, J. Electroanal. Chem. 769 (2016) 53–61. https://doi.org/10.1016/j.jelechem.2016.03.010.

49. A Döner, R Solmaz, M Özcan, G Kardaş, Experimental and theoretical studies of thiazoles as corrosion inhibitors for mild steel in sulphuric acid solution, Corros. Sci. 53 (2011) 2902–2913. https://doi.org/10.1016/j.corsci.2011.05.027.
50. I. Pawlaczyk, L. Czerchawski, W. Pilecki, E. Lamer-Zarawska, R. Gancarz, Polyphenolic-polysaccharide compounds from selected medicinal plants of Asteraceae and Rosaceae families: Chemical characterization and blood anticoagulant activity, Carbohydr. Polym. 77 (2009) 568–575. https://doi.org/10.1016/j.carbpol.2009.01.030
51. X. Li, S. Deng, H. Fu, Inhibition of the corrosion of steel in HCl, H2SO4 solutions by bamboo leaf extract. Corros. Sci. 62 (2012) 163–175. https://doi.org/10.1016/j.corsci.2012.05.008.
52. X. Lu, J. Wang, H.M. Al-Qadiri, C.F. Ross, J.R. Powers, J. Tang, B.A. Rasco, Determination of total phenolic content and antioxidant capacity of onion (Allium cepa) and shallot (Allium oschaninii) using infrared spectroscopy. Food Chemistry, 129 (2011), 637–644. https://doi.org/10.1016/j.foodchem.2011.04.105.
53. R. Sabzi, R. Arefinia, Investigation of zinc as a scale and corrosion inhibitor of carbon steel in artificial seawater. Corros. Sci. 153 (2019) 292–300. https://doi.org/10.1016/j.corsci.2019.03.045.
54. D.D. Joshi, UV–Vis. Spectroscopy: Herbal Drugs and Fingerprints, in Herbal Drugs and Fingerprints: Evidence Based Herbal Drugs, Springer India, India, 2012, pp. 101–120.
55. X. Zeng, Z. Du, Z. Sheng, W. Jiang, Characterization of the interactions between banana condensed tannins and biologically important metal ions (Cu^{2+}, Zn^{2+} and Fe^{2+}), Food Res. Int. 123 (2009) 518–528. https://doi.org/10.1016/j.foodres.2019.04.064.
56. X. Zeng, Z. Du, Y. Xu, Z. Sheng, W. Jiang, 2019. Characterization of the interactions between apple condensed tannins and biologically important metal ions [Fe^{2+} (3d6), Cu^{2+} (3d9) and Zn^{2+} (3d10)]. LWT. 114, 108384. https://doi.org/10.1016/j.lwt.2019.108384
57. L.L. Liao, S. Mo, J.L. Lei, H.Q. Luo, N.B. Li, Application of a cosmetic additive as an eco-friendly inhibitor for mild steel corrosion in HCl solution, J. Colloid Interface Sci. 474 (2016) 68–77. https://doi.org/10.1016/j.jcis.2016.04.015.
58. H.H. Hernández, A.M. Ruiz Raynoso, J.C. Trinidad Gonzalez, C.O. Gonzales Moran, J.G. Miranda Hernandez, A. Mandujano Ruiz, J.M. Hernandez, R.O. Cruz,

Electrochemical impedance spectroscopy (EIS): A review study of basic aspects of the corrosion mechanism applied to steels, in: M. El-Azazy, M. Min, P. Annus (Eds.) Electrochemical Impedance Spectroscopy, IntechOpen, London, 2020: p. 137–144.

59. P. Bommersbach, C Alemany-Dumont, J.P. Millet, B. Normand, Formation and behaviour study of an environment-friendly corrosion inhibitor by electrochemical methods, Electrochim. Acta, 51 (2005) 1076–1084. https://doi.org/10.1016/j.electacta.2005.06.001.
60. N. Ochoa, G. Baril, F. Moran, N. Pébère, Study of the properties of a multi-component inhibitor used for water treatment in cooling circuits, J. Appl. Electrochem. 32 (2002). 497–504. https://doi.org/10.1023/A:1016500722497.
61. S. Akbarzadeh, B. Ramezanzadeh, G. Bahlakeh, M. Ramezanzadeh, 2019. Molecular/elec tronic/atomic-level simulation and experimental exploration of the corrosion inhibiting molecules attraction at the steel/chloride-containing solution interface. J. Mol. Liq. 296, 111809. https://doi.org/10.1016/j.molliq.2019.111809.
62. R. Oltra, N. Pébère, B. Normand, Mesure de la corrosion: De la conceptualisation à la méthodologie, Presses polytechniques et universitaires romandes, Lausanne, 2016.
63. H. Zhang, N. Du, S. Wang, Q. Zhao, W. Zhou, 2020. Determination of iron valence states around pits and the influence of Fe^{3+} on the pitting corrosion of 304 stainless steel. Materials. 13, 726. https://doi.org/10.3390/ma13030726.
64. Z. Bai, K. Xiao, P. Dong, C. Dong, D. Wei, X. Li, Effect of iron ion diffusion on the corrosion behavior of carbon steels in soil environment, RSC advances, 8 (2018), 40544–40553. https://doi.org/10.1039/c8ra08032a.